https://doi.org/10.1016/j.jweia.2016.01.007

CFD simulation of the effect of an upstream building on the inter-unit dispersion in a multi-story building in two wind directions

D.J. Cui[a], C.M. Mak[a]*, K.C.S. Kwok[b] and Z.T. Ai[a]

[a] Department of Building Services Engineering,

The Hong Kong Polytechnic University, Hong Kong, China

[b] Western Sydney University, Penrith 2751, Australia

*Corresponding Author: E-mail: cheuk-ming.mak@polyu.edu.hk (C.M. Mak)

Tel.: +852 2766 5856 Fax: +852 2765 7198

Abstract

Previous studies on inter-unit dispersion are limited to isolated buildings. The influence of an upstream interfering building may significantly modify the indoor airflow characteristics of the wind-induced natural ventilated downstream interfered building. Motivated by the findings in previous studies, namely that infectious respiratory aerosols exhausted from a unit can re-enter into another unit in the same building through building envelope openings, this study investigates the inter-unit pollutant dispersion around a multi-story building in two wind directions by employing the computational fluid dynamics (CFD) method. The CFD model employed in this study has been validated against previous experimental data. The results show that the presence of an upstream building greatly changes the path lines around the downstream target building and the pollutant transportation routes around it. The presence of a low upstream building also greatly increases the average air exchange rate (ACH) values and the pollutant re-entry ratios (R_k) below the source unit on the windward side of the downstream target building for normal wind incidence. However, the presence of a high upstream building greatly increases the average ACH

values on the windward side and increases the R_k on the leeward side of the downstream building for oblique wind incidence.

Keywords:

Natural ventilation, Upstream building, Inter-unit dispersion, Wind directions, CFD

1 Introduction

Apart from outdoor air pollutants, airborne pollutants released from an indoor environment may also re-enter to adjacent units through open windows, posing a risk of infection, as occurred in the cross-transmission of Severe Acute Respiratory Syndrome (SARS) in Hong Kong in the spring of 2003 (Li et al., 2004). In densely populated urban areas like Hong Kong, residential buildings usually have a single opening to achieve single-sided natural ventilation. A large number of studies have been conducted based on models with this type of natural ventilation to investigate the mechanisms of indoor pollutant transportation between two units in the same building due to both buoyancy and wind effect (Li et al., 2004; Niu and Tung, 2008; Ai et al., 2013; Ai and Mak, 2014; Ai and Mak, 2015a; Cui et al., 2014).

Li et al. (2004) conducted a detailed analysis of the airborne transmission route in the residential estate Amoy Garden, where the largest number of SARS case occurred. They found that: (a) airborne viruses have high infection rates between adjacent units in residential buildings due to the quick evaporation of droplets in dry climate flu season; (b) the virus transportation route depends greatly on the airflow in the vicinity of buildings. Niu and Tung (2008) conducted an on-site measurement in a Hong Kong residential building to examine inter-unit pollutant transmission under buoyancy effect. They found that the re-entry ratio (R_k, defined in Section 3) of pollutants released from a source unit to the unit immediately above it reached up to 7%, which indicates the importance of vertical inter-unit dispersion. Ai and Mak (2014) studied inter-unit dispersion around multi-story buildings under different wind directions using the computational fluid dynamics (CFD) method. They found that inter-unit dispersion could occur along any

direction, namely upward, downward, and lateral directions. In particular, the units on the floor immediately below the source on the windward side, and vertically above it on the leeward side, where the R_k of rooms are up to 4.8% and 14.9% respectively, should be included in the high infection list.

Previous studies regarding inter-unit dispersion are limited mostly to isolated buildings. Given that almost all buildings in urban areas are surrounded by many other buildings, the effect of interference from surrounding buildings (e.g. Hajra et al., 2011) on the inter-unit dispersion is worthy of investigation. Many studies on urban airflow have been conducted based on metropolises, where buildings are tall and slender, with similar tall buildings in close proximity (Vardoulakis et al., 2003; Li et al., 2006; Hang et al., 2012; Tominaga et al., 2008). These studies reveal that the presence of proximity surrounding buildings dramatically reduces the air exchange rate (ACH) and pollutant exchange rate (PCH) around buildings (Ai and Mak, 2015b; Vardoulakis et al., 2003). Among surrounding buildings, the influence of an upstream building on its downstream building was paid particular attention, as it reduces significantly the external wind speeds (Zhang and Gu, 2008; Tominaga and Stathopoulos, 2011; Chang and Meroney, 2003) and curtails the pollutant dispersion around the downstream building (Hajra et al., 2011). The dimensions of an upstream building, especially its height, directly determine the size of the recirculation zone in the wake (ASHRAE, 2007; Fackrell and Pearce, 1981). However, previous studies regarding two upstream-downstream buildings focus mainly on the external airflow and pollutant dispersion around buildings, whereas the indoor airflow and pollutant dispersion were paid less attention.

This study investigates the effect of a proximity upstream building on the natural ventilation performance and inter-unit dispersion of a downstream building using CFD method. In practice, wind direction is a very important factor affecting airflow and dispersion around buildings (Johnson and Hunter, 1999). In this study, two wind directions, namely normal incidence and oblique incidence, were investigated. Similar to previous studies, this study focuses only on scenarios with single-sided natural ventilation.

2 CFD simulations

2.1 CFD methods

The CFD method has been widely used to predict airflow and pollutant dispersion in and around buildings (e.g. Ai et al., 2013; Blocken et al., 2008). In order to investigate the airflow characteristics and pollutant dispersion around residential buildings, Fluent 13.3 is used to predict the flow pollutant concentration fields in and around buildings. A modified, non-standard k-ε turbulence model, which offers a good compromise between accuracy and numerical cost, is applied (Montazeri and Blocken, 2013; Ai et al., 2013; Tominaga and Stathopoulos, 2007; Hargreaves and Wright, 2007). The time-averaged governing equation for an incompressible fluid can be written in the general form as Equation 1 below:

$$\frac{\partial}{\partial_t}(\varphi) + \nabla(u\varphi) = \nabla(\Gamma_\phi \nabla_\phi) + S_\phi \quad (1)$$

where u (m/s) is the velocity vector; φ stands for each of the velocity components, u (m/s), v (m/s), w (m/s), turbulent kinetic energy k (m^2/s^2), turbulent dissipation rate ε (m^2/s^3), and specious concentration c (g/m^3); Γ_Φ is the diffusion coefficient for each dependent variable φ; and S_φ is the source term.

The standard k-ε model is a semi-empirical model based on the model equations for turbulence kinetic energy (k) and its dissipation rate (ε). The turbulent viscosity, μ_t, is computed by combining k and ε as follows.

$$\mu_t = \rho C_\mu \frac{k^2}{\varepsilon} \quad (2)$$

where, ρ (kg/m^3) is the fluid density and C_μ is a model constant equal to 0.085. In the derivation of the standard k-ε model, the assumption is that the flow is fully turbulent, and the effects of molecular viscosity are negligible. The re-normalization group (RNG) k-ε model provides better predictions of flow field than the standard k-ε model, partially due to the term R_ε added to the ε equation, which improves the accuracy for swirling flow. In the ε equation, the added term R_ε is given by the equation below:

$$R_{\varepsilon} = \frac{C_{\mu}\rho\eta^{3}(1-\eta/\eta_{0})}{1+\beta\eta^{3}}\frac{\varepsilon^{3}}{k} \quad (3)$$

where, $\eta = Sk/\varepsilon$, η_0 and β are constants equal to 4.38 and 0.015, respectively. A tracer gas, CO_2 (carbon dioxide), is used to represent the pollutant and track its dispersion. The Species Transport model (Fluent, 2010) can predict the local mass fraction of each species. The Turbulent Schmidt number (Sc_t) is defined as the ratio of turbulent momentum diffusivity (eddy viscosity) (V_t) and turbulent mass diffusivity (D_t) ($Sc_t = V_t / D_t$). It is very important to solve the transport mass equation of the RANS model in CFD (Tominaga and Stathopoulos, 2007). Depending on the flow problem, the Sc_t value is usually treated as a constant ranging from 0.2-1.3 (Ai and Mak, 2013; Blocken et al., 2008; Hang et al., 2012). Previous studies employing the RNG model used the default number of Sc_t in Fluent (2010a), namely 0.7 (Ai et al., 2013), found that the numerical results have a good agreement with the experimental results. All simulations in this study set the Sc_t at 0.7.

2.2 Validation of interfering building

Zhang and Gu (2008) conducted atmospheric boundary layer wind tunnel measurements of wind-induced surface pressure on the facades of a residential building under the effect of a staggered interfering building (see Figure 1). The wind tunnel is 14 m long and has a cross-section area of 3.0 × 2.0 m^2. The atmospheric boundary layer is generated by a combination of long fetch of upwind terrain, with spires and roughness elements on the floor. As shown in Figure 1, the Downstream target building (solid line) and the upstream interfering building (dashed line) employed in the experiment have 0.01 m × 0.01 m square sections and the same height (H = 0.6 m).

Based on the best practice guidelines proposed by Franke et al. (2007), a computational domain with an upstream distance of 5H, downstream distance of 15H, lateral distance of 5H, and height of 6H is chosen. The mesh of 2.08 million cells consists of a hybrid grid with prismatic and hexahedral cells (see Figure 2). As each wall-adjacent cell's centroid should be located in the logarithmic layer when employing a

standard wall function, the near-wall $y+$ value should range between 30 and 300 (Fluent, 2010b). The $y+$ values in the vicinity of the building surfaces and domain ground in this validation are all between 30 and 40.

Considering the roughness of the ground, the velocity inlet employs a power law with a power law exponent $\alpha = 0.16$ (see Equation 4) and the reference velocity V_{ref} is set as 14.5 m/s at the height of Z_{ref} = 0.6 m, as in the experiment of Zhang and Gu (2008). Hence:

$$V_z = V_{ref}\left(Z / Z_{ref}\right)^{\alpha} = 15.73 V_{ref} Z^{0.16} \tag{4}$$

where V_z (m/s) is the wind speed at the vertical height Z (m).

Table 1 summarizes the boundary conditions used in the present validation study. Note that similar boundary conditions were used in previous studies (Ai et al., 2011a and 2011b, Gao et al., 2008). The same boundary velocity profile, but different turbulence profiles, was used in the CFD works of the experimenters (Zhang and Gu, 2008), which are also presented later to compare with the present simulations. Assuming that the flow is fully developed at the domain outlet, which means zero normal gradients and zero background pressure, the "pressure outlet" is selected. For domain top and lateral sides, slip boundary conditions are adopted. For the domain ground and building surfaces, no-slip boundary conditions combined with standard wall functions are adopted. Two 3D steady RANS turbulence models, standard k-ε and RNG k-ε, are adopted in the validated simulation. The SIMPLE algorithm is used for pressure-velocity coupling, pressure interpolation is second-order, and second-order discretization schemes are used for both the convection and viscous terms of the governing equations. Convergence is assumed to obtain when all the scaled residuals level off and reach a minimum of 10^{-6} for x, y, z momentum, and 10^{-5} for k, ε, and continuity. In their wind tunnel experiment, Zhang and Gu (2008) measured the pressure coefficient along the center line on walls S and N of the downstream target building. The dimensionless number pressure coefficient (C_p) is defined by Equation 5 below:

$$C_P = (P - P_r) / 0.5\rho v^2 \quad (5)$$

where P (P_a) is the measured surface pressure, P_r (P_a) is the reference pressure, ρ (kg/m^3) is the air density equal to 1.225 kg/m^3, and v (m/s) the mean wind speed at roof level.

A comparison of mean C_p between the CFD and wind tunnel results is shown in Figure 3. Compared to the experimental data, the average deviations of the C_p values produced by the standard k-ε model and the RNG model are 28.57% and 6.21%, respectively, on the windward side, and -12.08% and -19.19% on the leeward side. Obviously, the results of the RNG model have better agreements with the wind tunnel data. Moreover, the RNG model produces a more accurate recirculation zone in the wake of the target building than the standard *k-ε* model. The better performance of RNG model over the original standard model can be attributed to the many improvements built in the RNG model (Murakami and Mochida, 1988; Chavez et al., 2011). In addition, the C_p values predicted in the present study are closer to those predicted by the experimenters (Zhang and Gu, 2008), which indicates that the boundary conditions used are generally acceptable. Note that this validation compares only the results on the windward and leeward facades asthis paper focuses on the ventilation and pollutant dispersion through openings on the windward and leeward facades. Overall, this validation justifies the use of these selected numerical methods (RNG model) in the later simulations of airflow and inter-unit dispersion around two buildings.

3 Configuration descriptions

When encountering an isolated flat-roofed building, the urban wind will either deflect over the top, down in front, or around the sides (shown in Figure 4a). Due to the air pushing against the building, much of the windward wall will have relatively high pressure and the maximum pressure will occur at 70%-80% of the height of the building, where the wind is brought to a standstill in stagnation zones (Oke, 1978). When meeting with sharp corners, the accelerating flow will produce a below-atmosphere pressure area over the top, down in front, and around the sides, and the pressure difference will induce vortex and recirculation zones.

The length of the leeward recirculation zone (L_r) can be calculated based on the building dimensions using the equations in Table 2. D_s and D_l are the building dimensions that are perpendicular to the wind direction. D_s represents the length of the smaller edge and D_l the length of the larger edge. For two building cases, the downstream building's air flow pattern will be greatly affected when it is located in the leeward side recirculation zone (Figure 4b) of the upstream building, as the reverse flow in the leeward recirculation may cause the pollutant released from one unit to re-enter into adjacent units.

In order to study the effect of an upstream building on the wind-induced inter-unit dispersion around multi-story buildings, a 1:20 scale downstream target building and an upstream interfering building are adopted. Two rectangular boxes without openings are employed as the upstream building whose dimensions are shown in Figure 5a (Dash line). The downstream building has two independent units on each floor, with their openings facing the windward side (named W) and the leeward side (named L) (see Figure 5c). The unit dimensions are: width (D_x) × length (D_y) × height (D_z) = 6 m × 3 m × 3 m, and opening: width (D_x) × height (D_z) = 1 m × 2 m, in the prototype. The window bottom is 1 m above each floor.

The dimensions of the downstream target building in the prototype are $D_x \times D_y \times D_z$ = 6 m × 6 m × 12 m. Two upstream interfering building heights are considered, namely one equal to D_z and another equal to $2D_z$. The distance between the two buildings equal to the width of the building (6 m in prototype) which is smaller than the leeward recirculation length (see Table 2) of both high and low upstream buildings. A series of similarity criteria should be satisfied in order to reproduce the original full-scale flow. Geometric similarity and boundary layer flow similarity are relatively easy to achieve when appropriate scaled model, computational domain, and boundary conditions are selected. The computational domain for all the cases is a rectangular box surrounding the target building (see Figure 5) to simulate the natural ventilation, and the domain boundaries are sufficient to achieve the correct airflow around the buildings with the same ratio as the validation in Section 2.2.

Meroney's (2004) detailed review of the Reynolds number R_e ($R_e = V_{ref} D_z/\nu$) under purely wind-induced conditions indicated that the turbulent flow would be similar at all high Reynolds numbers greater than a threshold of 15,000. In addition, for the modeling of plumes interacting with structures, the similarity criteria are affected by source location, building orientation, and measurement location. The non-dimensional pollutant concentration distributions on a building surface could vary with wind speed until the R_e is larger than 3,000. In this work, the wind speed at the height of building roof is 4 m/s, resulting in a R_e of at least 4×10^4. This R_e is much larger than the threshold value suggested by Meroney (2004), suggesting that Reynolds independence is fulfilled.

Niu and Tang (2008) concluded that under the condition with an indoor-and-outdoor difference of 3 to 5 °C and a wind speed above 0.9 m/s, the thermally driven force of pollutant dispersion in the current building configurations can be ignored. Furthermore, natural ventilation is usually adopted in the seasons when the indoor-and-outdoor temperature difference is small. Thus, this study only considers the wind effect on natural ventilation and pollutant dispersion. Six cases are built to study the effect of an upstream building on the inter-unit dispersion of the downstream target building under different wind directions (see Table 3).

This study selects two wind directions as shown in Figure 5b; α is the angle between wind direction and the normal to the building surface. Each case is built independently, each with a dedicated computational domain. The arrangement of the buildings is shown in Figure 5a. The wind profile in an urban environment is determined by the following equation (Etheridge and Sandberg, 1996):

$$V_z = V_{ref} V (H/D_z)^{\alpha} = 1.14 V_{ref} Z^{0.25} \quad (6)$$

The turbulence at the inlet boundary is characterized by turbulence intensity and length scale, which are 8% and 1 m respectively. Air exchange rate (ACH) of each unit was calculated using an integral method: $\mathrm{ACH} = 3600 \times (0.5 \int_0^A |V_x|\, dA)/Vol_R$, where V_x (m/s) is the normal-to-opening velocity component, A

(m^2) the area of the opening, and Vol_R (m^3) the volume of each unit. The tracer gas CO_2 is released at a rate of 8 mg/s in the middle of each unit at a height of 1.6 m. The governing equation of this tracer gas is solved only after the convergence of flow field. Previous studies (Niu and Tung, 2008; Ai and Mak, 2014) used the re-entry ratio (R_k) to evaluate the inter-unit contamination, which is defined as:

$$R_k = M_{i-j}\,(Vol_j(ACH)_j / Vol_i(ACH)_i) \quad (7)$$

where M_{i-j} is mass fraction, which is the ratio of concentration at an infected unit (C_j, kg/m^3) to concentration at the source unit (C_i, kg/m^3).

A mesh with 4.2 million cells was employed after a mesh sensitivity test similar to that described in the validation section. Three types of meshes, namely coarser, medium and finer, were constructed for Case 1 (isolated building), which contains 2.1 million, 4.2 million and 6.5 million cells, respectively. The number of cell at the opening is 100, 200 and 300 for the three types of mesh, respectively. The average ACH values of the 4 units on the windward side predicted using the three types of mesh are 17.5, 16.2 and 16.4, respectively, and 14.1, 15.8 and 15.9 for the leeward side. It can be seen that the ACH values predicted by the medium mesh are very close to those predicted by the finer mesh, with a deviation less than 3%. Compromising between numerical cost and accuracy, the medium mesh was employed in this study.

4 Results and discussion

4.1 Airflow characteristics

The distance between the two buildings D_y (6 m) is smaller than L_r, as shown in Table 2. Figure 6 shows path lines on the vertical center plane of the computational domain. The air flow path lines of an isolated building (see Figure 6a) are basically similar to those in Figure 4. Influenced by the upstream buildings, air mainly flows downward near the windward side of the downstream target building because of the presence of a low upstream building (Figure 6b). Such a change in the near-wall flow pattern implies that the presence of a low upstream building may have an effect on the inter-unit pollutant dispersion route.

For example, when pollutants are released from the stagnation area, their transportation route will follow the air flows and change from downward and upward into all downward.

Figure 7 shows the air flow streamlines on the horizontal plane at the breathing level on the third floor of the downstream target building (Z = 0.37 m) for each case. For an isolated building, air flows separately into the lateral side, which means that the pollutant released from the windward units will be diluted quickly (Figure 7a). However, the presence of the upstream buildings causes two recirculation zones to occur on the windward side of the downstream building as it is located in the leeward cavity of the upstream buildings (Figure 7b, Figure 7c). In addition, the high upstream building has a larger recirculation than the low upstream building, which extended to the windward surface of the downstream target building (Figure 7c), but there is no dominant flow in the vertical direction (Figure 6c). This implies that the presence of a high upstream building induces more horizontal transportation of pollutants. In order to evaluate the effect of upstream buildings on the pollutant transportation route, the pollutant R_k will be calculated and discussed in Section 4.3.

As shown in Figure 8, under the effect of an upstream building, the mean velocity and turbulence kinetic energy fields around the downstream target building have changed, which means that the near-wall flow pattern has changed significantly. The presence of upstream buildings will induce more low-speed areas and significantly change the turbulent kinetic energy in the area between it and the downstream target building. However, in the vicinity of the downstream target building's windward wall (at around 1/8 D_y adjacent to the downstream building), the velocity magnitude is not significantly reduced by the presence of an upstream building.

The velocity profiles at two locations between the upstream building and downstream target building are presented in Figure 9. Figure 9a shows the profile at the mid-section between the two buildings, while Figure 9b shows the profile at 1/8 D_y from the downstream building. It can be seen that the velocity magnitudes at the mid-section (Figure 9a) are greatly reduced, by 75%, under the effect of an upstream

building (Case 2 and Case 3), compared to those in Case 1 with no upstream building. However, the velocity magnitudes at close proximity to the windward wall of the downstream building, as shown in Figure 9b, are relatively unaffected by the presence of an upstream building. The effects of an upstream building on the ventilation rate of every single unit in each case will be discussed further in Section 4.2.

4.2 Ventilation

Figure 10 shows the ACH for each unit for the six cases. W indicates a unit on windward side, and L on the leeward side. When wind direction is normal incidence, the presence of a low upstream building ($H = D_z$) significantly improves the ACH values of units W2, W3, and W4, especially for the top-most unit (W4), which is located above the stagnation area (70%-80% of the height of the target building). The presence of a high upstream building ($H = 2D_z$) in the same position has only a slight positive effect on the ACH values of each unit. On the leeward side, both low and high upstream buildings have a negative effect on ACH values.

When the wind direction is oblique (wind angle $\alpha = 45°$), the ACH values of all units are significantly better than under normal incidence wind direction (wind angle $\alpha = 0°$). Under an oblique wind, the presence of a low upstream building has a negative effect, decreasing the ACH value of all units on both windward and leeward sides, with the exception of W3. However, the presence of a high upstream building increased the ACH values by 140% on average on the downstream target building's windward side, but reduced the ventilation performance of all units on the leeward side (Table 4). The presence of a low upstream building undoubtedly influenced the ventilation performance of the downstream building.

From the results above, it can be seen that an upstream building and wind direction can totally change the indoor airflow characteristics. The location of a unit is also a very important parameter modifying the indoor ventilation performance. The results show that the presence of a low upstream building increases the ACH of the windward units under a normal incident wind, while the presence of a high upstream building increases the ACH value of windward units under an oblique incident wind (wind angle $\alpha = 45°$).

Under both wind directions, both types of upstream building reduce the ventilation performance for leeward units.

4.3 Pollutant dispersion

For wind-induced natural ventilation of a multi-story building, pollutant released from one unit may re-enter into other units of the building. Most buildings in cities like Hong Kong are high-rise cylinder-like buildings, which pose a risk of transporting pollutants between windward units and leeward units. The pollutant transportation characteristics of the six cases are discussed in this section. Figure 11 shows the pollutant re-entry ratio R_k for each case. R_k below 0.10% were regarded as negligible and are not shown. Figure 11 shows that the R_k from the windward source unit to the leeward units are higher than some of those from the source unit to the windward units. Therefore, R_k between the windward wall and the leeward wall are also calculated. Detailed observations are presented below.

4.3.1 Under normal wind incidence (α = 0°)

Pollutant source in Unit *W1*

When a pollutant is released from Unit W1 (see Figure 11a), the R_k of all units are negligible (R_k < 0.10%) in the case of an isolated building. This is because the source unit is located at the bottom of a downward recirculation and the momentum of the downward flow transferred into the frontal and lateral flow vortices, which in turn dilutes the pollutant effectively.

This situation is greatly changed by the presence of a low upstream building due to the downstream target building being located in its leeward recirculation cavity. Unlike those around a slab-like building (Ai et al., 2013), for a cylinder-like building, the lateral flow is strengthened on horizontal planes, which induce more pollutants to re-enter into leeward units. As is shown in Figure 11a, the R_k of leeward units are relatively high. In addition, due to the presence of a low upstream building, all leeward units' R_k in Case 2

(with a low upstream building) are all much higher than those of Case 1 (isolated building). The largest R_k is 0.35% in L2 in Case 2. This result is consistent with the flow characteristics explained in Section 4.1.

As the height of the upstream building increased to twice the height of the downstream target building, the pollutant R_k in all leeward units decreased significantly (see Figure 11a). Overall, when a pollutant is released from a bottom unit, the presence of a low upstream building induces large pollutant R_k, whilst a high upstream building will not have any obvious effect on the pollutant R_k.

Pollutant source in Unit *W2*

When the pollutant source of an isolated building is located in Unit W2, which is just below the stagnation area, the pollutant is mainly transported into the units below, due to the high pressure difference between the stagnation zone and its downward zone. As shown in Figure 11b, the R_k of Unit W1 reached 1.8% for the isolated building case. The presence of a low upstream building greatly increased the R_k (up to 15.16%) for Unit W1, which is the highest R_k for all cases. Meanwhile, the presence of a low upstream building also increases the R_k of leeward units in the downstream target building. However, when the upstream building is a high building, all units' R_k are greatly reduced (see Figure 11b). All leeward units' R_k are negligible.

Pollutant source in Unit *W3*

As mentioned in Section 4.1, due to the presence of a low upstream building, the air flow direction in the windward wall stagnation area of the downstream target building changes from separately downward and upward into all downward. When the pollutant source of an isolated building is located in the stagnation area (W3), the pollutant released from the source unit flows both upward and downward on the windward wall, which means that units W4 and W2 are both affected by the pollutant. However, the presence of a low upstream building changes the near-wall flow direction of the downstream target building. Owing to the recirculation vortex between the two buildings, the pollutant released from Unit W3 is mainly

transported downward. As shown in Figure 11c, owing to the presence of a low upstream building, the R_k of Unit W4 decreases from 0.15% to become negligible and the R_k of W2 and W1 is increased substantially from 0.30% and negligible to 6.76% and 8.32%, respectively, which is consistent with the flow characteristics introduced before. Similar to the windward wall, the presence of a low upstream building increases the R_k of leeward units. The presence of a low upstream building has a negative effect, which turns units W1 and W2 into very dangerous places, in terms of airborne disease control. However, when a high upstream building is present, the R_k of all units are negligible, with the exception of W4 and W2. Unit W2 is slightly affected by the high upstream building but the R_k of Unit W4 is increased greatly, from 0.15% to 9.90%. Overall, the presence of a high upstream building significantly increases the R_k of top-floor units on the windward wall.

Pollutant source in Unit W4

Lastly, when the pollutant source is located above the stagnation area (namely, Unit W4 in the downstream target building), the presence of a low upstream building significantly increases the R_k of the windward units, as the leeward recirculation cavity of the low upstream building induces the flow downwards (see Figure 11d). The presence of a low upstream building increased the R_k of Units W1, W2, and W3 from negligible to 6.46%, 3.92%, and 5.52%, respectively. Like the results on the windward wall, all leeward units' R_k are near or more than 2%. The largest R_k, 5.52%, occurs in Unit L4. The presence of a high upstream building does not have such a large negative effect. The R_k of all units, except Unit W2, are below 0.50% or negligible, and even that of W3 is only 1.15%.

4.3.2 Under oblique wind incidence (α = 45°)

When the wind direction changed from normal to oblique, R_k of all units decrease significantly due to the changed near-wall flow pattern. Under an oblique wind, there are two windward and two leeward walls on each building (see Figure 7d), which orient obliquely (α = 45°) to the incident wind but the basic pattern on the building's surfaces remains the same as that under the normal incidence wind (Oke, 1978).

When the wind approaches the buildings, it first reaches the sharp corners and then flows quickly around the leeward side. With such a flow pattern, the pollutant released from the windward units is quickly and effectively diluted into the flow streams. On the leeward sides, the pressure difference leads to two low-pressure recirculation zones, as show in Figure 7d. These recirculation zones may induce pollutants released from the windward units to re-enter into leeward units. As seen in the results of Case 4, Case 5, and Case 6 shown in Figure 11, under an oblique wind, the R_k of all windward units are negligible, no matter which unit the pollutants are released from. However, both low and high upstream buildings increase the pollutant R_k of units on the leeward side of the downstream target building.

When the pollutants are released from units W1, W3, and W4 of an isolated building, all leeward units' R_k are negligible. The presence of low upstream building increases the R_k of leeward units on the lower two floors (namely units L1 and L2). The presence of a high upstream building results in an increase of the R_k for all units, especially units L1 and L2. When the pollutant is released from Unit W2, the R_k of units L1 and L2 are larger than those of units L3 and L4. However, all R_k ratios are lower than 1%.

5 Conclusions

This study investigated the inter-unit dispersion around a multi-story building under the effect of an upstream building. The results show that the presence of an upstream building greatly changes the path lines of the downstream target building, which will change the pollutant transportation routes around the downstream building.

Existing knowledge tends to support the view that an upstream building will lower external wind speeds and then reduce the indoor ventilation performance of its downstream building. However, the results of the present study show that the presence of an upstream building does indeed induce a low-speed area between the upstream and downstream buildings, but does not necessarily reduce the wind speed in the vicinity of the downstream building.

A low upstream building increases greatly the average ACH values of the windward units of the downstream building for normal wind incidence. A high upstream building greatly increases the average ACH values of the windward units of the downstream target building for oblique wind incidence. However, this study has found that the presence of a low or high upstream building reduces the average ACH values of the leeward units of the downstream building for both normal and oblique wind.

Under normal wind incidence, the presence of a low upstream building greatly increases the pollutant re-entry ratio R_k for units below the source unit of the downstream target building on the windward side of the downstream building and slightly increases the R_k for most units on the leeward side of the downstream building. However, this study found that the presence of a high upstream building has a negligible effect on the R_k for all units on either the windward and leeward side of the downstream building.

Under oblique wind incidence, the main dispersion route of pollutants is from the windward side to the leeward side of the building. No matter which unit the pollutants are released from and whether it is an isolated building or a downstream target building under the influence of an upstream building (low or high), the R_k for all units on the windward side of the downstream building are negligible ($R_k < 0.10\%$). However, both low and high upstream buildings increase the pollutant R_k for units on the leeward side of the downstream building. A high upstream building also has a greater effect than a low upstream building in increasing R_k for most units on the leeward side of the downstream building.

The present study focuses on the influence of an upstream building on a downstream target building. When the interfering building is located downstream of the target building, it may strengthen the leeward reverse flow of the target building, which may induce higher pollutants R_k on the leeward side of the target building. Similarly, the presence of a lateral building may increase the wind speed of the flow on the lateral side of the target building and in turn influence pollutant dispersion. The effect of a downstream or lateral building on inter-unit pollutant dispersion will be the focus of future work. In

particular, more sophisticated computation models, such as large eddy simulation (LES) model, will be used to study the unsteady characteristics of inter-unit dispersion.

References

Ai Z.T., Mak C.M. 2013. CFD simulation of flow and dispersion around an isolated building: Effect of inhomogeneous ABL and near-wall treatment. Atmos. Environ. 77, 568-578.

Ai Z.T., Mak C.M. 2014. A study of inter-unit dispersion around multi-story buildings with single-sided ventilation under different wind directions. Atmos. Environ. 88, 1–13.

Ai Z.T., Mak, C.M. 2015a. Large eddy simulation of wind-induced inter-unit dispersion around multi-story buildings. Indoor Air. In Press, DOI:10.1111/ina.12200.

Ai Z.T., Mak, C.M. 2015b. From street canyon microclimate to indoor environmental quality in naturally ventilated urban buildings: issues and possibilities for improvement. Build. Environ. In Press, DOI: 10.1016/j.buildenv.2015.10.008.

Ai Z.T., Mak C.M., Niu J.L. 2013. Numerical investigation of wind-induced airflow and inter-unit dispersion characteristics in multi-story residential buildings. Indoor Air. 23, 417–429.

Ai Z.T., Mak C.M., Niu J.L., Li Z.R. 2011a. The assessment of the performance of balconies using computational fluid dynamics. Build. Serv. Eng. Res. Technol. 32(3), 229-243.

Ai Z.T., Mak C.M., Niu J.L., Li Z.R., Zhou Q. 2011b. Effect of balconies on ventilation performance of low-rise buildings. Indoor Built Environ. 20(6), 649-660.

ASHRAE. 2007. Building Air Intake and Exhaust Design. Chapter 44, ASHRAE Applications Handbook, Atlanta: American Society of Heating, Refrigeration and Air-Conditioning Engineers, Inc., Atlanta, USA.

Blocken B., Stathopoulos T., Saathoff P., Wang X. 2008. Numerical evaluation of pollutant dispersion in the built environment: comparisons between models and experiments. J. Wind Eng. Ind. Aerodyn. 96, 1817–1831.

Chang C.H., Meroney R.N. 2003. Concentration and flow distributions in urban street canyons: wind tunnel and computational data. J. Wind Eng. Ind. Aerodyn. 91, 1141–1154.

Chavez M., Hajra B., Stathopoulos T., Bahloul A. 2011. Near-field pollutant dispersion in the built environment by CFD and wind tunnel simulations. J. Wind Eng. Ind. Aerodyn. 99, 330–339.

Cui D.J., Mak C.M., Niu J.L. 2014. Effect of balconies and upper-lower vents on ventilation and indoor air quality in a wind-induced, naturally-ventilated building. Build. Serv. Eng. Res. Technol. 35, 393-407.

Etheridge D.W., Sandberg, M. 1996. Building ventilation: theory and measurement. Wiley, Chichester, UK.

Fackrell, J.E., Pearce, J.E., 1981. Parameters Affecting Dispersion in the Near Wake of Buildings CEGB Report RD/M/1179/N81.

Fluent. (2010a) ANSYS FLUENT 13.0 User's Guide, Modeling Turbulence, Canonsburg, PA, ANSYS Inc.

Fluent. (2010b) NSYS FLUENT 13.0 Theory Guide, Turbulence, Canonsburg, PA, ANSYS Inc.

Franke J., Hellsten A., Schlünzen H., Carissimo B. 2007. Best practice guideline for the CFD simulation of flows in the urban environment. Brussels: COST Office.

Gao, N.P., Niu, J.L., Perino, M. and Heiselberg, P. 2008. The airborne transmission of infection between flats in high-rise residential buildings: tracer gas simulation. Build. Environ. 43, 1805–1817.

Hajra B., Stathopoulos T., Bahloul A. 2011. The effect of upstream buildings on near-field pollutant dispersion in the built environment. Atmos. Environ. 45, 4930–4940.

Hang J., Li Y.G., Sandberg M., Buccolieri R., Sabatino S.D. 2012. The influence of building height variability on pollutant dispersion and pedestrian ventilation in idealized high-rise urban areas. Build. Environ. 56, 346–360.

Hargreaves D.M., Wright N.G. 2007. On the use of the k-ε model in commercial CFD software to model the neutral atmospheric boundary layer. J. Wind Eng. Ind. Aerodyn. 95, 355–369.

Johnson G.T. Hunter L.J. 1999. Some insights into typical urban canyon airflows. Atmos. Environ. 33, 3991-3999.

Li X.X, Liu C.H., Leung D.Y.C., Lam K.M. 2006. Recent progress in CFD modelling of wind field and pollutant transport in street canyons. Atmos. Environ. 40, 5640–5658.

Li Y., Duan S., Yu I.T.S., Wong T.W. 2004. Multi-zone modeling of probable SARS virus transmission by airflow between flats in Block E, Amoy Gardens. Indoor Air. 15, 96–111.

Meroney R.N. 2004. Wind tunnel and numerical simulation of pollution dispersion: A hybrid approach. Invited Lecture, Croucher Advanced Study Institute, Hong Kong University of Science and Technology, 6-10 December.

Montazeri H., Blocken B. 2013. CFD simulation of wind-induced pressure coefficients on buildings with and without balconies: validation and sensitivity analysis. Build. Environ. 60, 137–149.

Murakami S., Mochida A. 1988. 3-d numerical simulation of air flow around a cubic model by means of the k–ε model. J. Wind Eng. Ind. Aerodyn. 31, 283–303.

Niu J., Tung T.C.W. 2008. On-site quantification of re-entry ratio of ventilation exhausts in multi-family residential buildings and implications. Indoor Air. 18, 12–26.

Oke T.R. 1978. Boundary layer climates. Routledge, London.

Tominaga T., Mochida A., Yoshie R., Kataoka H., Nozu T., Yoshikawa M., Shirasawa T. 2008. AIJ guidelines for practical applications of CFD to pedestrian wind environment around buildings. J. Wind Eng. Ind. Aerodyn. 96, 1749–1761.

1 Tominaga Y., Stathopoulos T. 2007. Turbulent Schmidt numbers for CFD analysis with various types of
2 flow field. Atmos. Environ. 41, 8091–8099.

3 Tominaga Y., Stathopoulos T. 2011. CFD modeling of pollution dispersion in a street canyon:
4 comparison between LES and RANS. J. Wind Eng. Ind. Aerodyn. 99, 340–348.

5 Vardoulakis S., Fisher E.A.B., Pericleous K., Gonzalez-Flesca K., 2003. Modelling air quality in street
6 canyons: a review. Atmos. Environ. 37, 155–182.

7 Zhang A., Gu M. 2008. Wind tunnel tests and numerical simulations of wind pressures on buildings in
8 staggered arrangement. J. Wind Eng. Ind. Aerodyn. 96, 2067–2079.

Table and Figure Captions

Table 1. Boundary conditions for atmosphere boundary layer (ABL).

Table 2. Equations of different methods for calculating L_r.

Table 3. Cases configuration.

Table 4. Average ACH of four units on the windward and leeward sides.

Fig. 1. Schematic diagram showing relative location of buildings.

Fig. 2. Mesh information of near-building area.

Fig. 3. Mean pressure coefficient comparison of CFD and wind tunnel results.

Fig. 4. (a) Airflow pattern around a bluff body; (b) Schematic of the recirculation cavity zone on the leeward side of a bluff body (Oke, 1978).

Fig. 5. Computational domain and geometry of downstream target building.

Fig. 6. Air flow streamlines on the vertical center plane.

Fig. 7. Air flow streamlines on the horizontal plane at a height of Z = 0.37 m.

Fig. 8. Turbulent kinetic energy and mean velocity magnitude at the vertical center plane. (a) and (d): Case 1; (b) and (e): Case 2; (c) and (f): Case 3.

Fig. 9. Velocity profiles between two buildings. (a) Mid-section between two buildings; (b) Adjacent to downstream target building.

Fig. 10. ACH (h^{-1}) for Case 1 to 6. (a) Normal wind incidence angle (α=0º); (b) Oblique wind incidence angle (α=45º).

Fig. 11. Re-entry ratios (R_k) of tracer gas from the source to other units on leeward side. Red dot: tracer gas source; ① = Case 1; ② = Case 2; ③ = Case 3; ④ = Case 4; ⑤ = Case 5; ⑥ = Case 6 (a) Pollutants released from Unit W1; (b) Pollutants released from Unit W2; (c) Pollutants released from Unit W3; (d) Pollutants released from Unit W4

Table 1 Boundary conditions for atmosphere boundary layer (ABL)

	Power-law type (validation work)	Power-law (Zhang and Gu, 2008)
Domain inlet	$U = U_H \left(\frac{z}{z_H}\right)^{0.16}$ $I = 8\%$ $l = 0.6\,m$	$U = U_H \left(\frac{z}{z_H}\right)^{0.16}$ $k = \frac{3}{2}(uI)^2$ $\varepsilon = c_\mu k^{3/2}/l$
Domain outlet	$\frac{\partial}{\partial x}(u, v, w, k, \varepsilon) = 0$	
Domain ceiling	$w = 0,\ \frac{\partial}{\partial z}(u, v, k, \varepsilon) = 0$	
Domain lateral sides	$v = 0, \frac{\partial}{\partial z}(u, w, k, \varepsilon) = 0$	
Domain ground	wall functions (y^+ within 30~300)	
Building surfaces	non-slip for wall shear stress	
Turbulence coefficients	$C_\mu = 0.085,\ \eta_0 = 4.38, \beta = 0.015, \kappa = 0.42,$ E=8.331,	

Table 2 Equations of different methods for calculating L_r

Methods	Equation	L_r (m) (Case 2)	L_r (m) (Case 3)
ASHRAE (2007)	$L_r = D_s^{0.67} D_l^{0.33}$	7.5	9.7
Fackrell and Pearce ,1981	$L_r = \frac{1.8 D_y}{\left[\left(\frac{D_x}{D_z}\right)^{0.3}(1 + 0.24 D_y/D_z)\right.}$	11.9	15.4

Table 3. Cases configuration

	Case 1	Case 2	Case 3	Case 4	Case 5	Case 6
Arrangement of buildings	Isolated building	Upstream building ($H = D_z$)	Upstream building ($H = 2D_z$)	Isolated building	Upstream building ($H = D_z$)	Upstream building ($H = 2D_z$)
Wind direction (α)	0°	0°	0°	45°	45°	45°

Table 4 Average ACH of four units on the windward and leeward sides

	Case 1	Case 2	Case 3	Case 4	Case 5	Case 6
Windward ACH (h^{-1})	16.2	38.9	20.7	56.6	43.5	125.2
Leeward ACH (h^{-1})	15.8	11.3	14.8	42.8	36.4	17.7

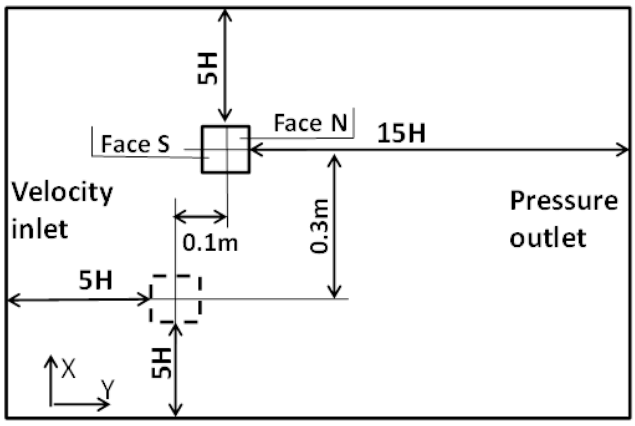

Fig. 1 Schematic diagram showing relative location of buildings

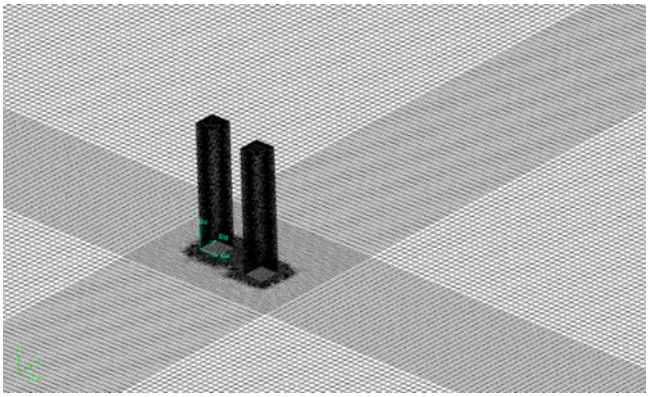

Fig. 2 Mesh information of near-building area

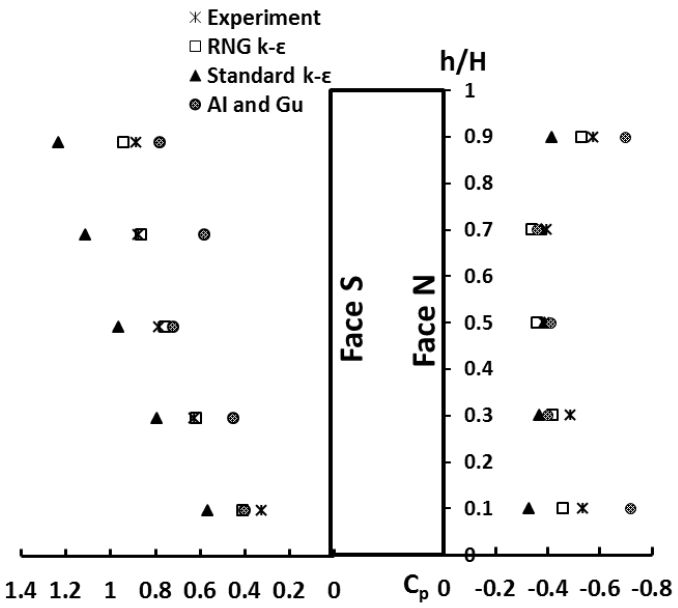

Fig. 3 Mean pressure coeffcient comparision of CFD and wind tunnel results

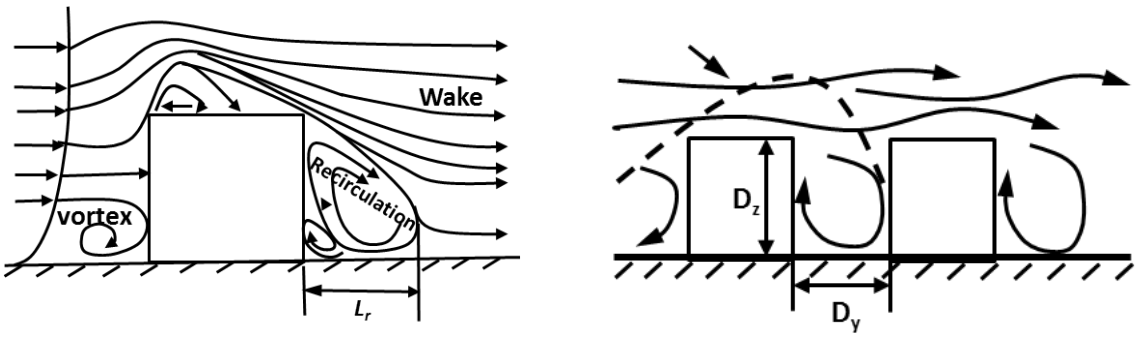

(a) (b)

Fig. 4 (a) Airflow pattern around a bluff body; (b) Schematic of the recirculation cavity zone on the leeward side of a bluff body (Oke, 1978)

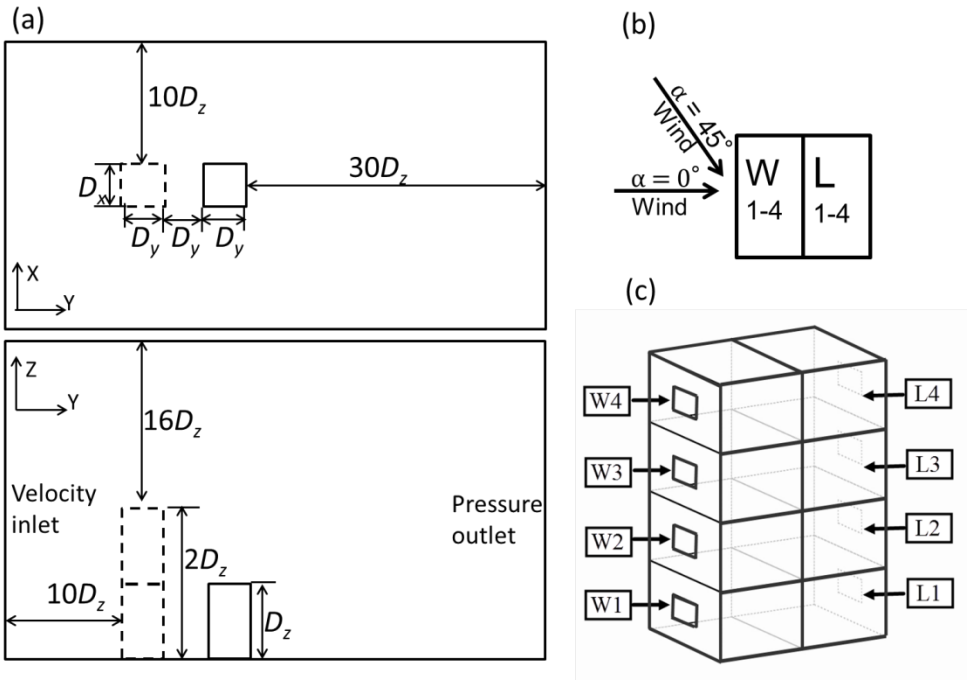

Fig. 5 Computational domain and geometry of downstream target building

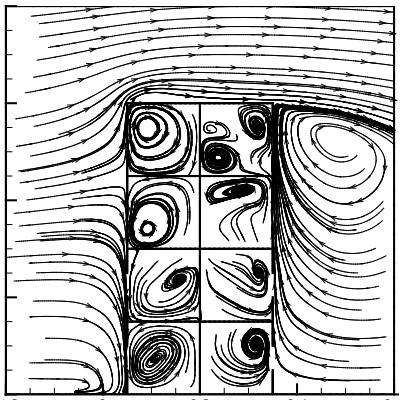

(a) Case 1

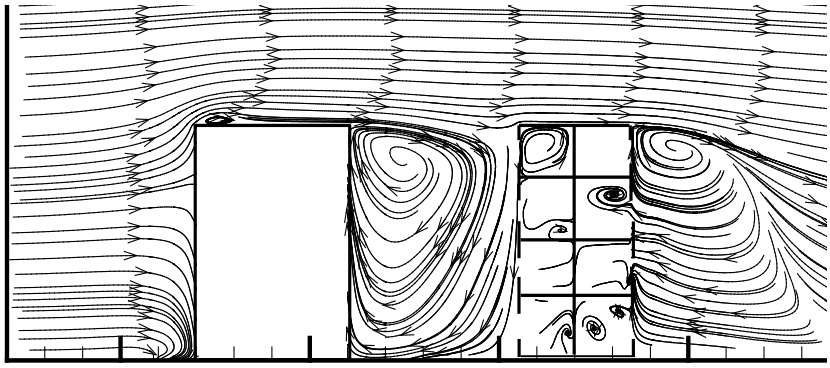

(b) Case 2

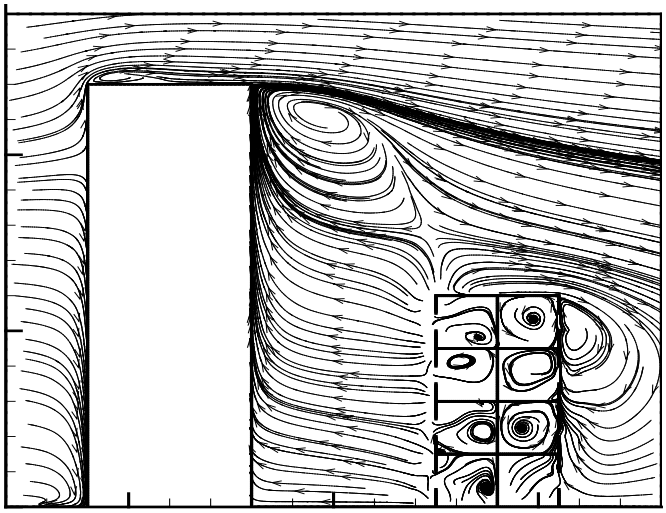

(c) Case 3

Fig. 6 Air flow streamlines at vertical center plane

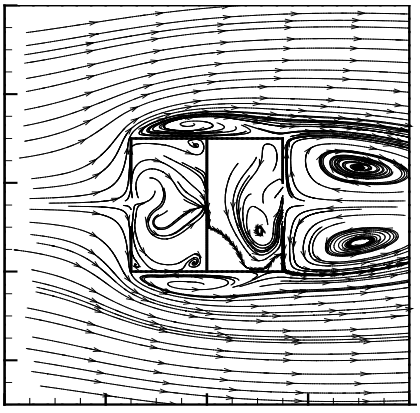

(a) Case 1

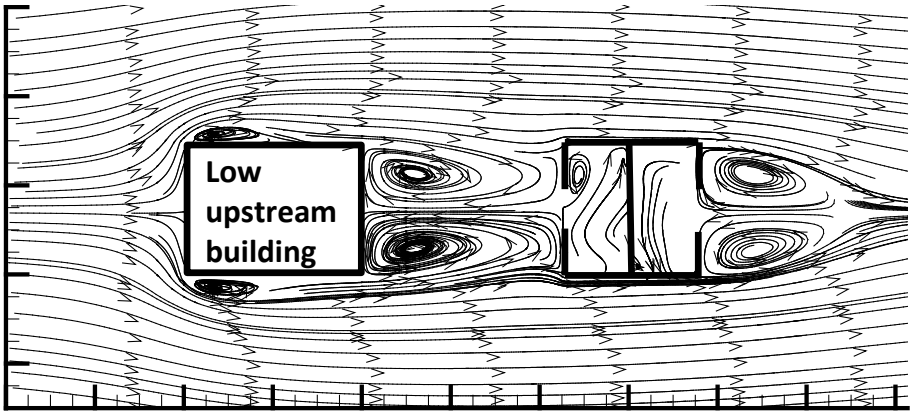

(b) Case 2

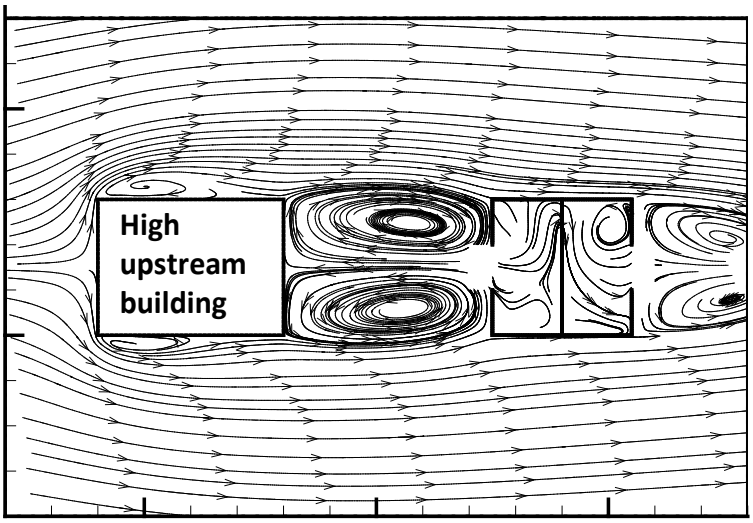

(c) Case 3

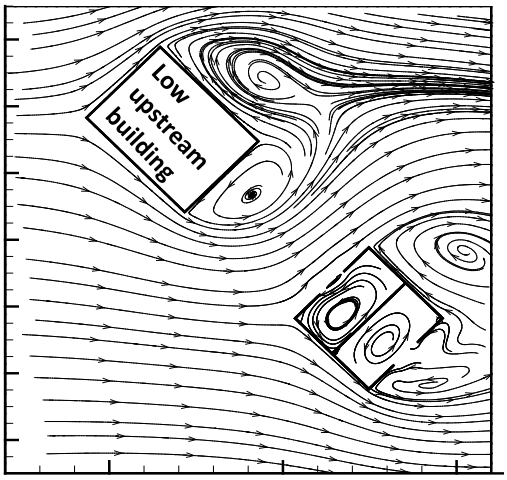

(d) Case 5

Fig. 7 Air flow streamlines on horizontal plane at a height Z = 0.37 m

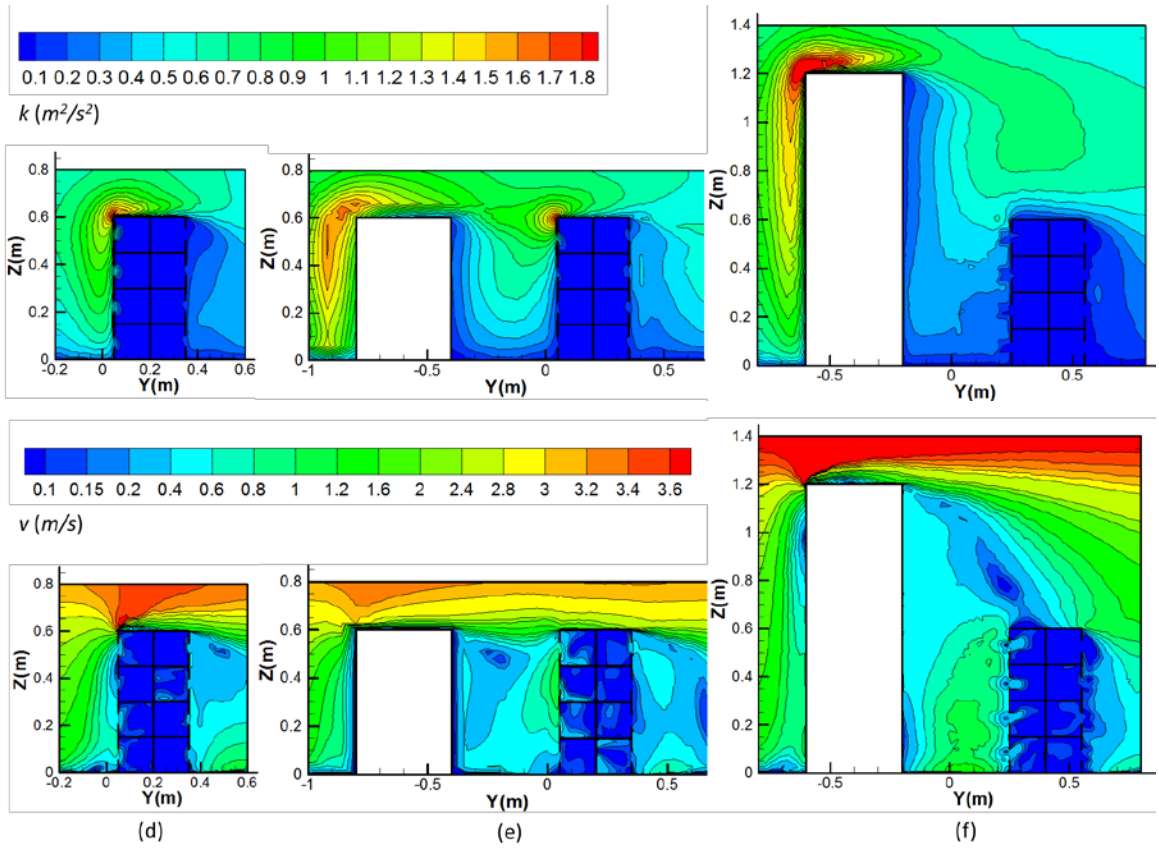

Fig. 8 Turbulent kinetic energy and mean velocity magnitude at vertical center plane. (a) and (d): Case 1; (b) and (e): Case 2; (c) and (f): Case 3

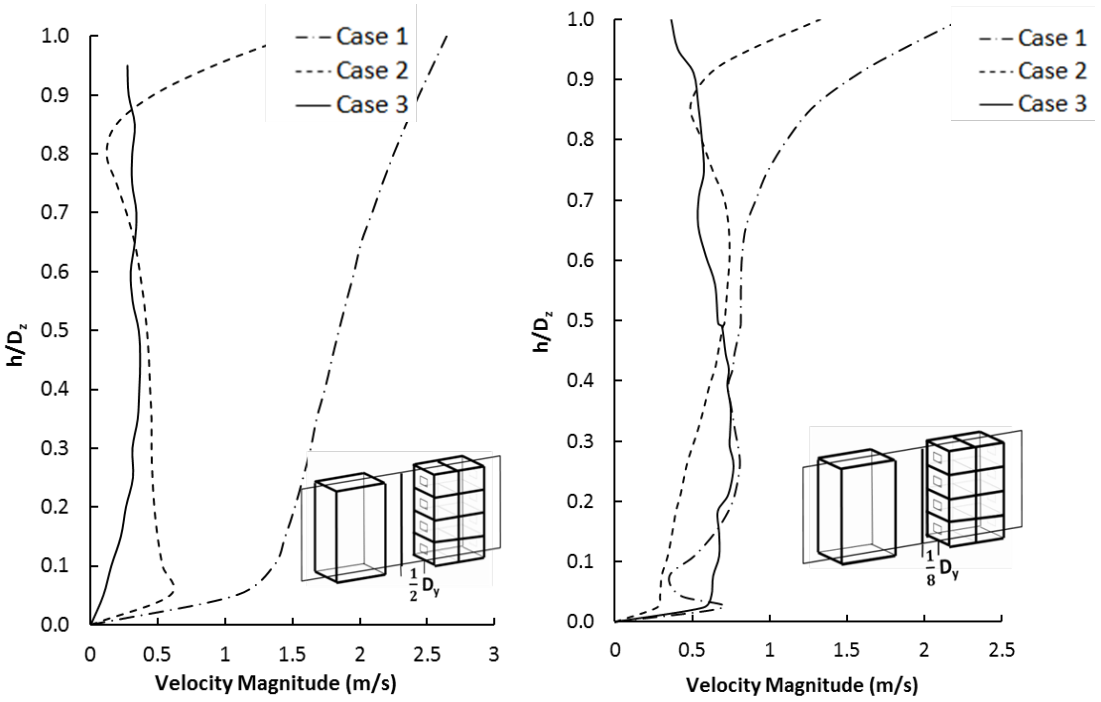

(a) Mid-section between two buildings (b) Adjacent to downstream target building

Fig. 9 Velocity profiles between two buildings

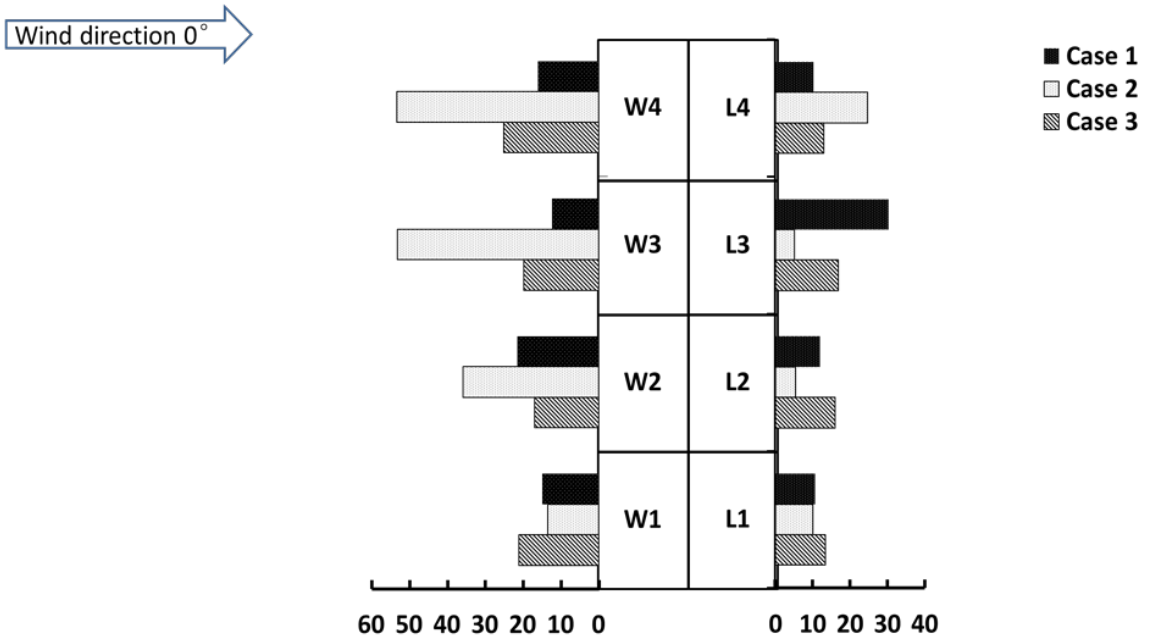

(a) Normal wind incidence angle (α=0º)

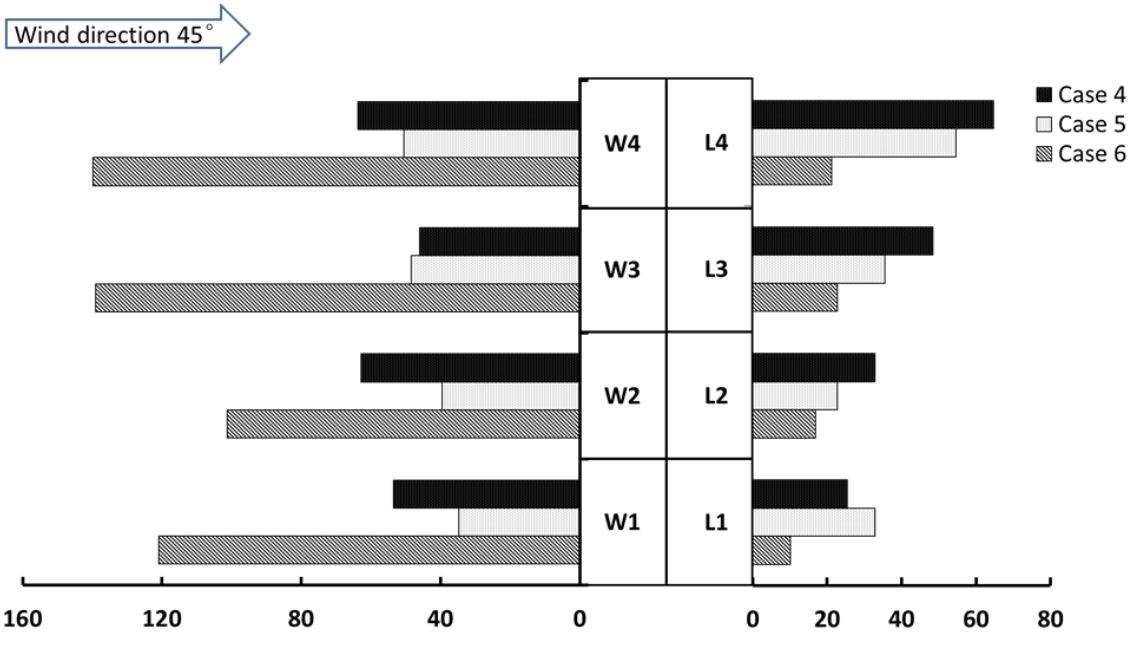

(b) Oblique wind incidence angle (α=45º)

Fig. 10 ACH (h^{-1}) for Cases 1 to 6

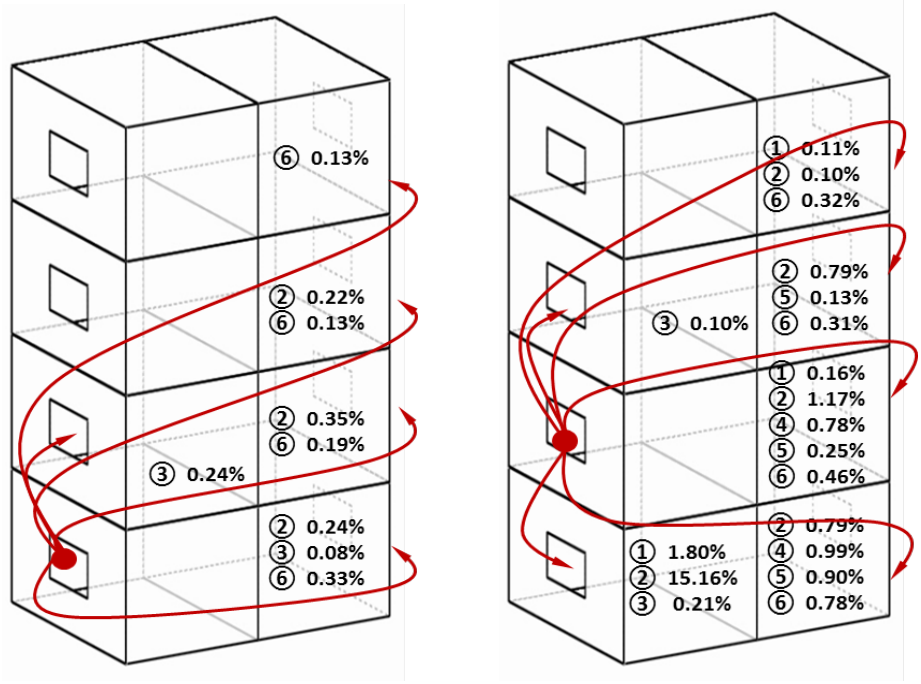

(a) Pollutants released from Unit W1 (b) Pollutants released from Unit W2

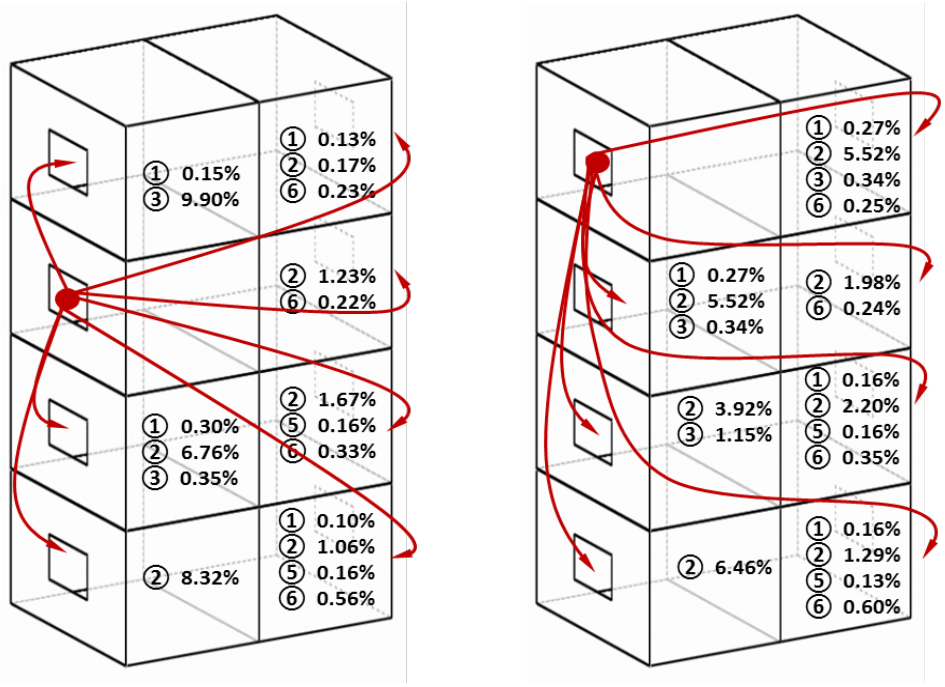

(c) Pollutants released from Unit W3 (d) Pollutants released from Unit W4

Fig. 11 Re-entry ratios (R_k) of tracer gas from the source to other units on leeward side. Red dot: tracer gas source; ① = Case 1; ② = Case 2; ③ = Case 3; ④ = Case 4; ⑤ = Case 5; ⑥ = Case 6